

The Supernova Remnant G296.7–0.9 in X-rays (Research Note)

T. Prinz¹ and W. Becker^{1,2}

¹ Max Planck Institute for extraterrestrial Physics, Giessenbachstrasse, 85741 Garching, Germany
e-mail: tprinz@mpe.mpg.de

² Max-Planck Institut für Radioastronomie, Auf dem Hügel 69, 53121 Bonn, Germany

Received ;date; / Accepted ;date;

ABSTRACT

Aims. We present a detailed study of the supernova remnant (SNR) G296.7–0.9 in the 0.2–12 keV X-ray band.

Methods. Using data from XMM-Newton we performed a spectro-imaging analysis of G296.7–0.9 in order to deduce the basic parameters of the remnant and to search for evidence of a young neutron star associated with it.

Results. In X-rays the remnant is characterized by a bright arc located in the south-west direction. Its X-ray spectrum can be best described by an absorbed non-equilibrium collisional plasma model with a column density of $N_{\text{H}} = 1.24^{+0.07}_{-0.05} \times 10^{22} \text{ cm}^{-2}$ and a plasma temperature of $6.2^{+0.9}_{-0.8}$ million Kelvin. The analysis indicates a remnant age of 5800 to 7600 years and a distance of $9.8^{+1.1}_{-0.7}$ kpc. The latter suggests a spatial connection with a close-by HII region. We did not find evidence for the existence of a young neutron star associated with the remnant.

Key words. ISM: supernova remnants - ISM: individual objects: G296.7–0.9 - Stars: neutron

1. Introduction

Every year, several hundred supernova (SN) events are observed, representing the end state of stellar evolution in which a core-collapse of a massive star or the thermonuclear disruption of a white dwarf takes place. SNe are the most energetic events which can be observed in the universe. They are often as bright as a whole galaxy. Their extreme brightness allows to see them up to distances of Gpc (Rodney et al. 2011). At this scale, though, the only information obtainable from them is the characteristic rising and fading of their light as a function of time, i.e. their photometric light-curve, and their spectral evolution, both of which are important for their classification (Sako et al. 2008). Most of these events are discovered in the optical band by comparing observations which were taken at different epochs.

In our own Galaxy the rate of observed SNe is small. For core-collapse supernovae it averages to only about two per century. This estimate is suggested by the γ -ray radiation from ^{26}Al in the Galaxy (Diehl et al. 2006) in which a certain yield is expected to be formed in each core-collapse SN. Many SNe, though, remain unobserved due to optical light extinction. The last recorded SN in our Galaxy, the Kepler SN, was observed in AD 1604 and not more than six other SNe have been detected in the Galaxy in the past two thousand years (Green & Stephenson 2003). The optical light from the two youngest Galactic SNe, G1.9+0.3 and Cas A, were not observed about 100 and 350 years ago (Reynolds et al. 2008; Green & Stephenson 2003).

If the direct light from a SN was missed, for several nearby ones we have the chance to study at least the light of their remnant, which remains visible in various spectral bands for up to 10^5 years. Although the light echo from the SN Cas A was found recently (Rest et al. 2008), it is one of the few cases so far where the SN light could be studied a few hundred years after the SN. The most promising way to learn about the evolution of a

SN shock front and the feedback on the evolution of their host galaxy is therefore to study the diffuse emission of SNRs.

In the last years several new SNRs have been detected thanks to the increasing sensitivity of modern X-ray observatories. One of those remnants is G296.7–0.9, which was first detected in X-rays by Schaudel et al. (2002) and later identified to be a SNR by Schaudel (2003) and Robbins et al. (2012). It is a shell-like SNR from which X-ray and radio emission has been detected. In addition, filaments in the infrared and $\text{H}\alpha$ band were detected in the near proximity of the source (Robbins et al. 2012). Whether they are associated with the remnant still remain to be shown.

A first detailed study of the SNR G296.7–0.9 was presented by Robbins et al. (2012) using ROSAT PSPC data. As this detector had roughly five independent energy channels in the range 0.1–2 keV, the spectral results deduced in their analysis were very limited. They suggested that the X-rays were emitted from a thermal plasma. Robbins et al. (2012) therefore were not able to put any constraints with high confidence on the derived spectral parameters. The ROSAT data did not allow them to deduce parameters like the age or the expansion velocity of the remnant.

In this work we report on an XMM-Newton observation which was targeted on SNR G296.7–0.9. The results of the spatial and spectral analysis of this data is presented in Section 2. A discussion is given in Section 3 in which we use the inferred spectral parameters of G296.7–0.9 to derive an estimate for its age, its radius, its expansion velocity and its distance. Section 4 provides the concluding summary.

2. X-ray observation and data reduction

G296.7–0.9 was observed for 13.6 ksec on 28 June 2011 with the EPIC cameras (Strüder et al. 2001) on board the X-ray observatory XMM-Newton (ObsID 0675070101). The two MOS and the PN cameras were operated in Full-Frame mode using the

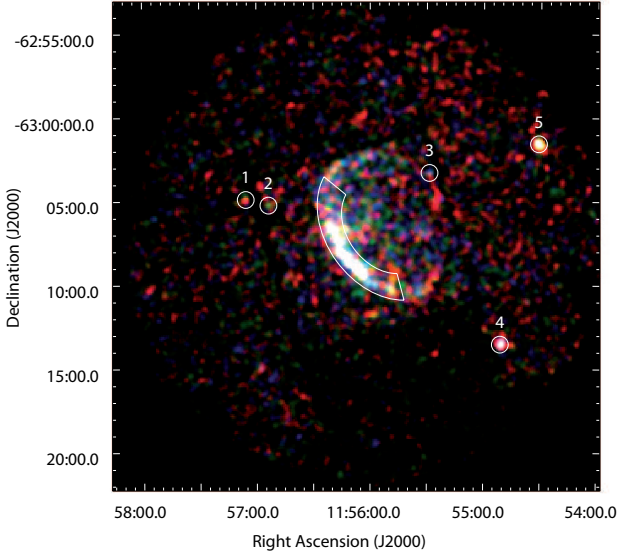


Fig. 1. $30' \times 30'$ XMM-Newton MOS1/2 color image of G296.7–0.9 (red 0.5–0.9 keV, green 0.9–1.3 keV and blue 1.3–2 keV). The superimposed images are binned with $6''$ per pixel and smoothed by a Gaussian kernel of $\sigma = 30''$ to enhance the visibility of the diffuse emission. The photons detected in the annular sector shown in white were used for spectral analysis of the supernova remnant.

medium filter. Part of the observation was taken with the filter wheel in closed position because the observation was strongly affected by particle background radiation. Therefore, the performed duration was only 4.4 ksec and 5.5 ksec for the PN and MOS1/2 detectors, respectively.

We used the XMM SAS version 11.0.0 to reprocess and reduce the data. Times of high background activity were identified by inspecting the light curves of the MOS1/2 and PN data at energies above 10 keV. After rejecting these times the effective exposures of the PN, MOS1 and MOS2 cameras were 3.7 ksec, 5.1 ksec, and 5.3 ksec, respectively. We extracted images and exposure maps in the five standard bands of XMM-Newton using all EPIC instruments. Single and double events were selected from the PN data and single to quadruple events from the MOS data sets.

For the spectral fitting we used the X-Ray Spectral Fitting Package (XSPEC) version 12.7.0u. and restricted the energy range to 0.4 – 6.0 keV because the count rate detected at higher energies was too sparse for a meaningful spectral analysis. Below 0.4 keV the detector and telescope response is not well established. All given uncertainties represent the 1σ confidence range for one parameter of interest, unless stated otherwise.

2.1. Spatial analysis

Figure 1 shows the X-ray color image of SNR G296.7–0.9. A bright arc that appears to lie along an elliptical shell is clearly detected in the south-east. Its center is at $RA_c = 11^h55^m52^s.3 \pm 0^s.7$, $DEC_c = -63^\circ06'29'' \pm 3''$ with a semi major axis of $5'$ and a semi minor axis of $3'.75$.

We searched for point sources with a signal-to-noise ratio S/N of at least 3σ in the five standard bands using a sliding box source detection algorithm (SAS tool `edetect_chain`). Five point sources were detected (see Fig. 1), which all have a $S/N \geq 7\sigma_G$ ($\sigma_G = 1 + \sqrt{c_{bg} + 0.75}$, where c_{bg} are the background counts).

Table 1. Detected sources in XMM-Newton observation 0675070101. The sources are denoted as in Fig. 1.

No.	RA (J2000) h:m:s	DEC (J2000) d:m:s	S/N σ_G	Rate cts/ksec
1	11 : 57 : 05.7 \pm 0.3	-63 : 04 : 53 \pm 2	7.7	5.2
2	11 : 56 : 53.9 \pm 0.3	-63 : 05 : 13 \pm 2	8.5	5.7
3	11 : 55 : 28.6 \pm 0.3	-63 : 03 : 18 \pm 2	7.0	4.1
4	11 : 54 : 51.2 \pm 0.3	-63 : 13 : 31 \pm 2	34.1	26.4
5	11 : 54 : 31.1 \pm 0.3	-63 : 01 : 33 \pm 2	22.2	16.4

Their position, positional error, signal-to-noise ratio and count rate in the merged image are listed in Table 1.

In order to search for optical counterparts we cross-correlated the position of each X-ray source with the various online catalogs provided by the VizieR service¹. We found a candidate counterpart for source #5, HD 103442 (Høg et al. 2000), which is an A3/4IV star with an optical magnitude $V = 8.8$. Its angular separation from source #5 is $4''.0$, corresponding to twice the observatory’s absolute astrometric accuracy². The source density ρ in this region of the Galactic plane using the Tycho-2 catalog is $\rho \approx 0.09$ arcmin⁻². The probability of a chance association computes then like $P_{\text{coin}} = \rho \cdot \delta^2$, where δ is the angular separation between the optical and X-ray source. For the optical counterpart of source #5 we compute a chance probability of 4×10^{-4} for a mis-identification. Its X-ray flux within the 0.3 to 3.5 keV band is 1.2×10^{-12} erg cm⁻² s⁻¹, yielding an X-ray to visual flux ratio of $\log(f_X/f_V) = -3.1$. This is in the allowed range of -3.86 ± 0.79 for A-type stars (Maccacaro et al. 1988; Agüeros et al. 2009) which further strengthens the association between source #5 and its candidate optical counterpart.

No source has been detected close to the geometrical center of the SNR. Using the merged MOS1/2 data we determined a 3σ upper limit on the count rate of a hypothetical central X-ray source of 4.3×10^{-3} cts/s in the energy range 0.2 to 12 keV.

2.2. Spectral analysis

The energy spectrum of G296.7–0.9 was extracted from an elliptical annular sector with the center at RA_c and DEC_c , semi major axes of $5'$ and $2'.9$, semi minor axes of $3'.75$ and $2'.2$ and an opening angle of 140° . The background spectrum was derived from a nearby region placed on the same MOS1/2 chip with the same size as the source region. The background contribution was found to be $\approx 50\%$ in the two MOS cameras and $\approx 71\%$ in the PN data. After subtracting the background 1232, 1236, and 3077 source counts remained in the MOS1, MOS2, and PN data. For the spectral analysis of the remnant these counts were binned to have at least 75 counts per bin in the case of the MOS1/2 observations and 150 counts per bin for the PN data.

We checked whether the spectral fitting results would change if we model the instrumental background according to the suggestions made by Kuntz & Snowden (2008). They proposed to add a Gaussian at the fluorescence line of Al $K\alpha$ at $E = 1.49$ keV with zero width and a power law for modeling the remaining soft proton contamination, which is not convolved with the instrumental response. As it turns out from this analysis the model fits were not significantly better than without adding these components using the standard F-test. Thus, the following results are without modeling the instrumental background separately.

¹ <http://vizier.u-strasbg.fr/viz-bin/VizieR>

² xmm.vilspa.esa.es/docs/documents/CAL-TN-0018.pdf.

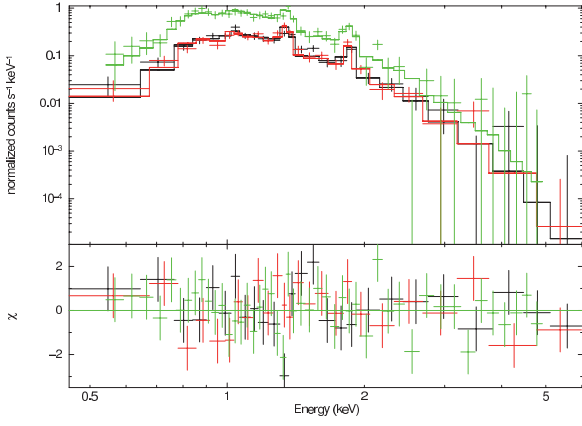


Fig. 2. Spectrum and fitted model (NEI) of the X-ray emission of SNR G296.7–0.9. The black colored line indicates the MOS1 data, the red the MOS2 and the green the PN data.

We fitted the spectrum of G296.7–0.9 with various models: A hot diffuse gas model (MEKAL), a model for a collisionally ionized diffuse gas (APEC), a power law model, a thermal bremsstrahlung model, a Raymond-Smith diffuse gas model, a non-equilibrium collisional plasma that allows a temperature evolution (GNEI) or has a constant temperature (NEI, see Figure 2), a plane-parallel shock plasma model (PSHOCK), an ionization equilibrium collisional plasma model (EQUIL), and a Sedov model with separate ion and electron temperatures. For spectral models with $\chi^2_{\text{red}} < 1.4$, all fit parameters are listed in Table 2.

In the following, we will use the best-fit results of the NEI model to derive related SNR parameters. For all models with a non-equilibrium equation of state we measure an ionization timescale value $\tau = t_0 n_e < 10^{12} \text{ s cm}^{-3}$ (t_0 is the age of the remnant and n_e the post-shock electron number density), which is smaller than the expected timescale at which collisional ionization equilibrium is reached (Borkowski et al. 2001). Therefore, the APEC and EQUIL model are unlikely to apply. For the GNEI model the temperature and the ionization timescale-averaged temperature are almost the same, which is no improvement over the NEI model. Additionally, we will not use the results of the SEDOV model any further, because the determination of the postshock temperature T_e in that model is only possible at energies above 3 to 4 keV (Borkowski et al. 2001) where the spectrum of G296.7–0.9 is not well constrained.

The value for N_H in the NEI model fit is slightly lower than the average integrated hydrogen column density toward SNR G296.7–0.9, which is $N_H^{LAB} = 1.39 \times 10^{22} \text{ cm}^{-2}$ (Kalberla et al. 2005). This value is based on HI emission line measurements at a radio frequency of 21 cm and refers to the entire hydrogen column density along the line of sight. The temperature of the plasma is $6.2^{+0.9}_{-0.8} \times 10^6 \text{ K}$. No improvement in the best-fit statistic was observed when we allowed the abundances to differ from the solar values. Using the derived parameters of the NEI model fit the flux in the 0.5 to 4 keV band is $5.2^{+1.1}_{-0.9} \times 10^{-11} \text{ erg/cm}^2/\text{s}$.

In addition we investigated the spatial variation of the spectral parameters by extracting all photons in the northern and southern part of the remnant. However, no difference was found within the derived errors.

3. Discussion

3.1. Comparison with the ROSAT results

Schaudel (2003) and Robbins et al. (2012) independently analyzed two pointed ROSAT PSPCB observations. These data were taken between 1st and 8th of February 1993 and 19th and 21st of February 1998. Both authors found the temperature of the X-ray emitting gas and the hydrogen column density N_H lower by at least a factor of two when compared with the results deduced in our work. Only Schaudel (2003) found a N_H which is comparable with our value listed in Table 2 by fitting the Raymond-Smith model, though his value had a much higher uncertainty. As already mentioned in the introduction, the PSPCB had about five independent energy channels, which limits the conclusions drawn from their spectral fits, especially when 70 spectral bins were used as in the work of Robbins et al. (2012). The latter corresponds to an oversampling of about 15 times the spectral resolution of the detector!

3.2. Supernova remnant

Using the deduced spectral parameters from the NEI fit we can derive basic properties of the remnant, such as the distance d , post-shock hydrogen density n_H , swept-up mass M , the age of the remnant t , the radius in pc R_s , and the shock velocity v_s .

We used the following set of equations, which is described in detail in Prinz & Becker (2012) and references therein.

$$\begin{aligned}
 d_{\text{Sedov}} &= 7420 \cdot \theta^{-3/5} \left(\frac{E_{51}}{T_s} \right)^{2/5} \left(\frac{f}{\text{Norm}} \right)^{1/5} \text{ [kpc]} \\
 d_{\text{Reddening}} &= N_H / (N_H / A_V \cdot A_V / E_{B-V} \cdot E_{B-V} / \text{kpc}) \text{ [kpc]} \\
 V_{\text{emit}} &= 3.029 \times 10^{54} \cdot f \cdot \theta^3 \cdot (d_{\text{Sedov}} [\text{kpc}])^3 \text{ [cm}^3\text{]} \\
 n_H &= 70.27 \sqrt{\frac{\text{Norm}}{d_{\text{Sedov}} \cdot f \cdot \theta^3}} \text{ [cm}^{-3}\text{]} \\
 M &= 1.4 \cdot n_H \cdot m_H \cdot V \text{ [kg]} \\
 t &= 2.71 \times 10^9 \left(\frac{E_{51}}{n_H} \right)^{1/3} T_s^{-6/5} \text{ [yr]} \\
 R_s &= 0.34 \left(\frac{E_{51}}{N_H} \right)^{1/3} t^{2/3} \text{ [pc]} \\
 v_s &= 0.4 \cdot R_s / t \text{ [km/s]}.
 \end{aligned}$$

Herein $\theta = \sqrt{\text{major} \times \text{minor axis}}$ is the reduced radius of the remnant in arcmin, E_{51} the explosion energy in units of 10^{51} erg , T_s the fitted plasma temperature, f the filling factor to correct for the morphology of the SNR, Norm the normalization of the spectral fit, N_H the fitted column density, V_{emit} the X-ray emitting volume, and m_H the mass of a hydrogen atom. The errors listed with the numbers deduced from these equations are statistical errors. The systematic errors might be larger but are unknown.

The Sedov-analysis based distance is $d_{\text{Sedov}} = 9.8^{+1.1}_{-0.7} \text{ kpc}$. In the following, we give all important quantities in units of $d_{9.8} = d/9.8 \text{ kpc}$ as d_{Sedov} has a smaller uncertainty than other distance estimates. From Figure 1 we infer that only $f = 15\%$ of the remnant is bright enough to be used for spectral analysis. Therefore, the post-shock hydrogen density N_H is $0.73^{+0.18}_{-0.10}$ and the swept-up mass is $M = 29 M_{\odot} d_{9.8}^{5/2}$. Assuming that the explosion energy E is equal to the canonical value of 10^{51} erg , the age of the remnant is 5800 to 7600 years and the radius is $R_s = 12.2^{+1.2}_{-0.8} d_{9.8}^{1/6} \text{ pc}$. We derive a shock velocity v_s of $720^{+130}_{-100} \text{ km/s}$.

Table 2. Spectral parameters of the best-fit models for SNR G296.7–0.9.

model	N_{H} [10^{22}cm^{-2}]	$k_{\text{B}}T$ [keV]	τ^{α} [10^{11}s/cm^3]	$k_{\text{B}}T_e^{\beta}/\langle kT \rangle^{\gamma}$ [keV]	Norm $^{\delta}$ [10^{-2}cm^{-5}]	$\chi^2/\text{d.o.f.}$	f_X^{ϵ} [$10^{-11} \text{erg cm}^{-2} \text{s}^{-1}$]
NEI	$1.24^{+0.07}_{-0.05}$	$0.53^{+0.08}_{-0.07}$	$1.2^{+0.8}_{-0.4}$	-/-	$1.3^{+0.6}_{-0.3}$	89.3/94	$5.2^{+1.1}_{-0.9}$
PSHOCK	$1.16^{+0.14}_{-0.06}$	$0.54^{+0.08}_{-0.06}$	8^{+15}_{-7}	-/-	$1.1^{+0.6}_{-0.2}$	87.5/94	$3.5^{+0.5}_{-0.3}$
SEDOV	$1.27^{+0.10}_{-0.09}$	$0.35^{+0.19}_{-0.08}$	6^{+7}_{-4}	< 0.54/-	$2.3^{+2.1}_{-0.9}$	89.4/93	8 ± 3
GNEI	1.27 ± 0.08	$0.49^{+0.11}_{-0.08}$	$1.0^{+0.8}_{-0.5}$	-/0.55 $^{+0.11}_{-0.08}$	$1.5^{+0.9}_{-0.6}$	88.6/93	$6.0^{+1.0}_{-1.5}$
EQUIL	1.10 ± 0.04	0.52 ± 0.04	-	-/-	$1.09^{+0.21}_{-0.15}$	96.8/95	2.5 ± 0.2
APEC	1.23 ± 0.05	$0.38^{+0.10}_{-0.03}$	-	-/-	$2.0^{+0.6}_{-0.5}$	107.0/95	$4.6^{+0.6}_{-0.5}$

Notes. $^{\alpha}$) ionization timescale $^{\beta}$) electron temperature immediately behind the shock front $^{\gamma}$) ionization timescale-averaged temperature $\langle kT \rangle = \int_{\tau_s}^{t_0} T(t)n_e(t)dt/\tau$ $^{\delta}$) Norm= $\frac{10^{-14}}{4\pi[D_A(1+z)]^2} \int n_e n_{\text{H}} dV$, where D_A is the angular diameter distance to the source in cm, n_e and n_{H} are the post-shock electron and hydrogen densities in cm^{-3} , respectively. $^{\epsilon}$) X-ray flux in the energy range 0.5 to 4.0 keV.

km/s. Using the flux values deduced in Section 2 we compute its luminosity to be $L_X^{0.5-4} = 6.0^{+1.8}_{-1.4} \times 10^{35} d_{9.8}^2 \text{erg/s}$.

Independently of the Sedov analysis another method which allows us to estimate the remnant’s distance makes use of a relation between the visible extinction A_V and the color excess: $A_V/E_{B-V} = 3.2 \pm 0.2$. The remnant’s color excess is not known, so that we use the distribution of the mean color excess E_{B-V} per kiloparsec derived by Lucke (1978). In the direction of the remnant we find $E_{B-V}/\text{kpc} = 0.25 \pm 0.10$. In addition, we used the relation between N_{H} and the visual extinction A_V of Predehl & Schmitt (1995) $N_{\text{H}}/A_V = (1.79 \pm 0.03) \times 10^{21} \text{cm}^{-2}$. This leads to a distance of $d_{\text{Reddening}} = 9 \pm 4 \text{kpc}$ which is in agreement with the distance deduced from the Sedov analysis. However, the mean color excess (E_{B-V}) which we used to calculate $d_{\text{Reddening}}$ was derived for a reddening layer up to 2 kpc and thus is just a rough estimate.

3.3. Compact central object

To obtain a rough estimate of the flux upper limit for a hypothetical compact source in the center of the remnant, we assumed that the source has properties similar to a Central Compact Object (CCO), because no compact source or radio pulsar has been detected in G296.7–0.9 so far (Robbins et al. 2012). Like other CCOs, e.g. the one in the SNR Puppis A, we assume that the spectrum is dominated by blackbody emission with a temperature of $\approx 2.6 \times 10^6$ Kelvin and a luminosity in the 0.5–10 keV band of at least 10^{32}erg/s (see Becker 2009, for a review). This corresponds to a flux in this energy range of $\approx 9 \times 10^{-15} \text{erg cm}^{-2} \text{s}^{-1}$. Using the WebPIMMS tool with the fitted N_{H} of the SNR the count rate in the 0.2–12 keV range is $> 2 \times 10^{-4} \text{cts/s}$ for the merged MOS1 and MOS2 observations, an order of magnitude lower than the derived 3σ upper limit for a point-like source at the center of the remnant. That we do not detect emission from a CCO in G296.7–0.9 does therefore not mean that there is none. The observation might not be deep enough to detect it. The type of the supernova is also unconstrained.

4. Conclusion and summary

The remnant is characterized by a bright arc in the south-west direction and by diffuse emission with low surface brightness in its western part. We showed that the X-ray emission of G296.7–0.9 is in agreement with coming from a collisionally heated plasma which has not reached equilibrium yet. The Sedov analysis leads to the conclusion that the SNR is about 6600 years old and is expanding with a velocity on the order of $\approx 720 \text{km/s}$.

The close-by HII region G296.593–0.975 has a velocity of $+25 \pm 1 \text{km s}^{-1}$ based on measured hydrogen recombination lines (Caswell & Haynes 1987). With the standard IAU parameter for the distance to the center of our Galaxy $R_0 = 8.5 \text{kpc}$ and the solar orbit velocity of $V_0 = 220 \text{km/s}$ derived by Kerr & Lynden-Bell (1986) and the Galactic rotation model of Fich et al. (1989) we deduce a distance to the HII region of $9.3 \pm 0.6 \text{kpc}$. For the error estimate we assumed an uncertainty in the velocity-to-distance conversion of 7km/s (e.g., Clifton et al. 1988).

The deduced distance d_{Sedov} is in good agreement with the distance of the close-by HII region G296.593–0.975. This is a strong indicator for a spatial connection between the SNR and the HII region as already suggested by Robbins et al. (2012).

The observation used in this analysis was strongly affected by particle background radiation, which led to a net observation time that was shorter by a factor of three than the approved exposure time. Therefore, only limited statements can be made about the existence of a compact source located near the center of the supernova remnant. Deeper observations might help to clarify this question and the one of the type of the SN in more detail.

Acknowledgements. We acknowledge the use of the XMM-Newton data archive. T.P. acknowledges support from and participation in the International Max-Planck Research School on Astrophysics at the Ludwig-Maximilians University.

References

- Agüeros, M. A., Anderson, S. F., Covey, K. R., et al. 2009, *ApJS*, 181, 444
Becker, W. 2009, in *Astrophysics and Space Science Library*, Vol. 357, Astrophysics and Space Science Library, ed. W. Becker, 91
Borkowski, K. J., Lyerly, W. J., & Reynolds, S. P. 2001, *ApJ*, 548, 820
Caswell, J. L. & Haynes, R. F. 1987, *A&A*, 171, 261
Clifton, T. R., Frail, D. A., Kulkarni, S. R., & Weisberg, J. M. 1988, *ApJ*, 333, 332
Diehl, R., Halloin, H., Kretschmer, K., et al. 2006, *Nature*, 439, 45
Fich, M., Blitz, L., & Stark, A. A. 1989, *ApJ*, 342, 272
Green, D. A. & Stephenson, F. R. 2003, in *Lecture Notes in Physics*, Berlin Springer Verlag, Vol. 598, *Supernovae and Gamma-Ray Bursters*, ed. K. Weiler, 7–19
Hög, E., Fabricius, C., Makarov, V. V., et al. 2000, *A&A*, 355, L27
Kalberla, P. M. W., Burton, W. B., Hartmann, D., et al. 2005, *A&A*, 440, 775
Kerr, F. J. & Lynden-Bell, D. 1986, *MNRAS*, 221, 1023
Kuntz, K. D. & Snowden, S. L. 2008, *A&A*, 478, 575
Lucke, P. B. 1978, *A&A*, 64, 367
Maccacaro, T., Gioia, I. M., Wolter, A., Zamorani, G., & Stocke, J. T. 1988, *ApJ*, 326, 680
Predehl, P. & Schmitt, J. H. M. M. 1995, *A&A*, 293, 889
Prinz, T. & Becker, W. 2012, *A&A*, 544, A7
Rest, A., Welch, D. L., Suntzeff, N. B., et al. 2008, *ApJ*, 681, L81
Reynolds, S. P., Borkowski, K. J., Green, D. A., et al. 2008, *ApJ*, 680, L41
Robbins, W. J., Gaensler, B. M., Murphy, T., Reeves, S., & Green, A. J. 2012, *MNRAS*, 419, 2623

- Rodney, S. A., Riess, A. G., Strolger, L., et al. 2011, in American Astronomical Society Meeting Abstracts #218, #219.01
- Sako, M., Bassett, B., Becker, A., et al. 2008, *AJ*, 135, 348
- Schaudel, D. 2003, PhD thesis, LMU, Germany
- Schaudel, D., Becker, W., Voges, W., et al. 2002, in Astronomical Society of the Pacific Conference Series, Vol. 271, Neutron Stars in Supernova Remnants, ed. P. O. Slane & B. M. Gaensler, 391
- Strüder, L., Briel, U., Dennerl, K., et al. 2001, *A&A*, 365, L18